Available online at www.sciencedirect.com
ScienceDirect
Trans. Nonferrous Met. Soc. China 35(2025) 2598−2611
Transactions of Nonferrous Metals Society of China
www.tnmsc.cn

Effect of electro-pulsing treatment on tensile properties and microstructure of SLM-produced TC4 alloy

Zhen-shang HU[1], Yi YANG[1], Ming-xia WU[1], Ling XUE[1], Qiang LI[1], Dong LU[2,3], Yong-sheng LIU[2,3]

1. School of Mechanical Engineering, Sichuan University, Chengdu 610065, China;
2. Sichuan Advanced Metal Material Additive Manufacturing Engineering Technology Research Center, Chengdu Advanced Metal Materials Industry Technology Research Institute Co., Ltd., Chengdu 610300, China;
3. State Key Laboratory of Vanadium and Titanium Resources Comprehensive Utilization, Pangang Group Research Institute Co., Ltd., Panzhihua 617000, China

Received 27 December 2023; accepted 22 August 2024

Abstract: The effect of electro-pulsing treatment (EPT) with different peak current densities (J_m) on tensile properties of selective laser melting (SLM)-produced TC4 alloy was investigated for significant improvement in the tensile properties of the alloy. When J_m is 30 A/mm^2, the elongation is improved distinctly by 19.72% while the ultimate tensile strength remains nearly constant. The improved ductility is evidenced by deeper dimples on the fracture surface and cracks from the shear lip zone. Additionally, the improvement is reflected by widely distributed voids and prominent slip bands in the longitudinal section of the fracture. The fracture behavior is attributed to the increased high-angle grain boundaries fraction and the reduced dislocation density induced by the appropriate EPT. This microstructure leads to a decrease in texture intensity of the basal plane and an enhancement in crystalline slip capacity of the plane, consequently, the improved plastic deformation capacity of the alloy.

Key words: electro-pulsing treatment; SLM-produced TC4 alloy; tensile properties; fracture behavior; microstructure

1 Introduction

TC4 alloy is known for its good lightweight properties, biocompatibility, and corrosion resistance [1]. The allotropy of titanium and the variety of associated microstructures make it ideal for selective laser melting (SLM), one of the most frequently used additive manufacturing techniques [2]. SLM has been widely applied in medical implants and aeronautical parts. These applications require the corresponding components to have high ultimate tensile strength (UTS) and yield strength [3].

However, TC4 alloy is of poor thermal conductivity, and there is a wide temperature gradient between the top melting layers and the cooler bottom layers during SLM [4]. These properties result in an uneven microstructure in the alloy [4]. Additionally, the deposition direction has been proven to affect the anisotropic mechanical performance of the SLM-produced TC4 alloy (SLMed TC4) [5]. SUN et al [5] reported that the UTS of the SLMed TC4 sample oriented at 0° was inferior to those of samples with orientations at 45° and 90°. Despite various efforts including scanning strategy modification and post-processing, some conventional post-treatments such as annealing and hot isostatic pressing failed to prevent grain growth in the alloy, which reduced its strength, and these treatments were time-consuming [6−9]. Remedies that can avoid the shortcomings have not yet been thoroughly investigated.

Corresponding author: Ming-xia WU, Tel: +86-28-85402279, E-mail: wumingxia@scu.edu.cn
https://doi.org/10.1016/S1003-6326(25)66835-X

Over the past two decades, electro-pulsing has attracted significant interest as an efficient and environmentally friendly treatment for modifying metals [10]. Numerous studies have focused on the mechanisms through which the current modifies the mechanical properties and microstructure of TC4 alloy. ROSS et al [11] investigated the effects of electro-pulsing on the bulk deformation of TC4 alloy under tensile and compressive loads. Their results indicated that electro-pulsing resulted in a pronounced ductility, with improvements far exceeding those achieved by resistive heating. GAO et al [12] discovered that short-term electro-pulsing treatment (EPT) enabled TC4 alloy to achieve superior dynamic ductility by transforming the bimodal microstructure into a typical lamellar microstructure. ZHAO et al [13] processed TC4 alloy using electro-plastic compression and found that the microstructural evolution and increased plasticity during the process were dominantly attributed to the thermal and athermal effects of electro-pulsing. These effects promoted the dislocation motion, enhanced the nucleation rate of dynamic globalization, and induced the $\alpha \rightarrow \beta$ phase transition. ZHAO et al [14] analyzed the influence of the electrical parameter duty cycle on the spring-back of TC4 alloy sheets during electrically assisted stretch U-bending tests, and found that a 30% duty cycle was optimal for reducing spring-back. GAO et al [15] realized the refinement and hardening of the microstructure of SLMed TC4 alloy with the applied voltage approaching 7.5 kV.

However, in those reports, EPT was primarily regarded as a forming technology for the TC4 alloy. A high current density in the treatment would lead to substantial energy consumption for the electro-pulsing device. In addition, systematic studies employing pulse current with low density to enhance the tensile property of the SLMed TC4 alloy have been scarce. Moreover, the specific tensile fracture behavior of the alloy has not been comprehensively studied.

Hence, the purpose of the current study is to utilize electro-pulsing with a relatively low current density to improve the resistance to tensile fracture in the SLMed TC4 alloy, where the deposition direction is perpendicular to the tensile direction. To this end, the optimal treatment was selected based on the UTS and elongation tested from samples subjected to different pulse current densities. Furthermore, the microstructure of the TC4 sample after EPT was characterized.

2 Experimental

The raw material was composed of spherical TC4 powder with an average powder particle size of approximately 50 μm (Fig. 1).

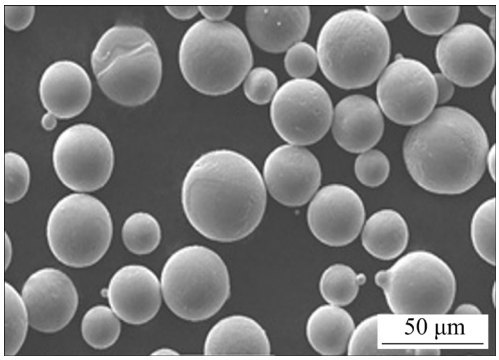

Fig. 1 Morphology of TC4 powder

The chemical composition (in mass fraction) was as follows: 0.0027% H, 0.0084% N, 0.01% C, 0.2068% O, 0.05% Fe, 4.43% V, and 5.86% Al, with the balance being Ti. The laser power was 280 W, the laser beam scanning velocity was 1200 mm/s, and the hatch distance was 0.14 mm. After the SLM process, the blanks were annealed at (800±14) °C for 2 h to relieve the warpage, followed by furnace cooling. According to ASTM B265—20a, they were processed into TC4 tensile samples, as shown in Fig. 2(a).

Figure 2(b) displays the diagram of the EPT. The sample was connected to two copper electrodes at both ends, which were connected to the generating device that produced a unidirectional square-form current. The waveform was specified by basic parameters, including the voltage (<10 V), pulse width (≤100 ms), and interval between pulses (1−999 ms). An AT−4204 multi-channel transducer was used to measure the temperature on the surface of the sample during electro-pulsing processing.

UTS, elongation, and stress−strain curves of the material were measured at room temperature and a strain rate of 2 mm/min. Subsequently, morphologies on the fracture surface and metallographic structures on the longitudinal section of the fracture were characterized by scanning electron microscopy (Phenom ProX, 15 kV, Secondary electron) for fracture behavior

analysis. Additionally, a microstructure analysis was conducted using optical microscopy and electron backscattered diffraction (EBSD) with a step size of 0.5 μm, focusing on the center of the section of each sample. To verify the evolution of the dislocation morphology in each sample, a transmission electron microscope (TEM, JEOL JEM F200, 200 kV, Bright field) analysis was performed.

In this work, the samples were grouped based on the peak current density (J_m). They were divided into six groups, labeled UT, EPT-1, EPT-2, EPT-3, EPT-4, and EPT-5, with the corresponding J_m values of 0, 10, 20, 30, 40, and 50 A/mm^2, respectively. The duration approached 4 s, with a pulse width of 100 ms, which was followed by air cooling. To ensure the reliability of the experimental results, four tensile samples were prepared for each group.

3 Results and discussion

3.1 Tensile properties

Figure 3 presents the UTS, elongation, and engineering stress−strain response of each sample treated via different pulse current densities.

When J_m is lower than 30 A/mm^2, the elongation continues increasing, while the UTS has no significant fluctuation. The variation of the UTS is less than 4%. When J_m increases to 30 A/mm^2, the elongation reaches its maximum value, increasing by 19.72% compared with that of the UT tensile sample. However, as J_m exceeds 30 A/mm^2, both the UTS and elongation decrease evidently. When J_m reaches 50 A/mm^2, UTS and elongation of the sample are the lowest. Therefore, EPT-3 is the optimal treatment, as it noticeably realizes the toughness improvement of the material.

3.2 Temperature evolution

Temperature was used to analyze the structural evolution with the influence of electro-pulsing and compare the energies provided by different pulse current densities [16]. As shown in Fig. 4, an increase in the current density J_m promotes the temperature rise rate and the terminal temperature.

It should be noted that the temperature of the EPT-5 sample increased nearly four times compared with that of the EPT-4 sample. The temperature rise is proportional to the square of current density [10]. Although the internal temperature is generally higher than the surface

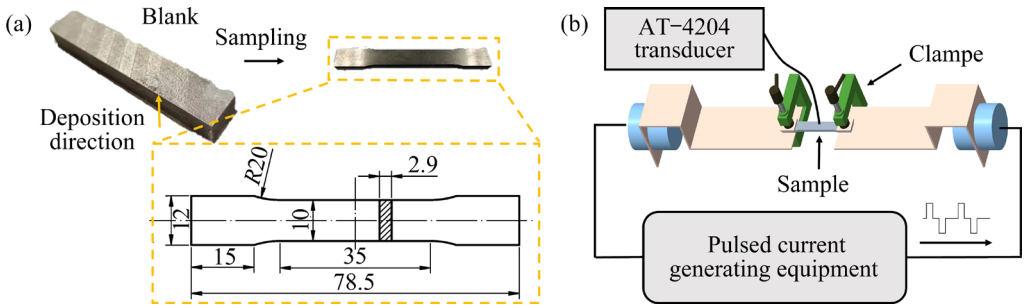

Fig. 2 Diagrams for machining of SLMed TC4 alloy (a) and experimental setup of EPT (b) (unit: mm)

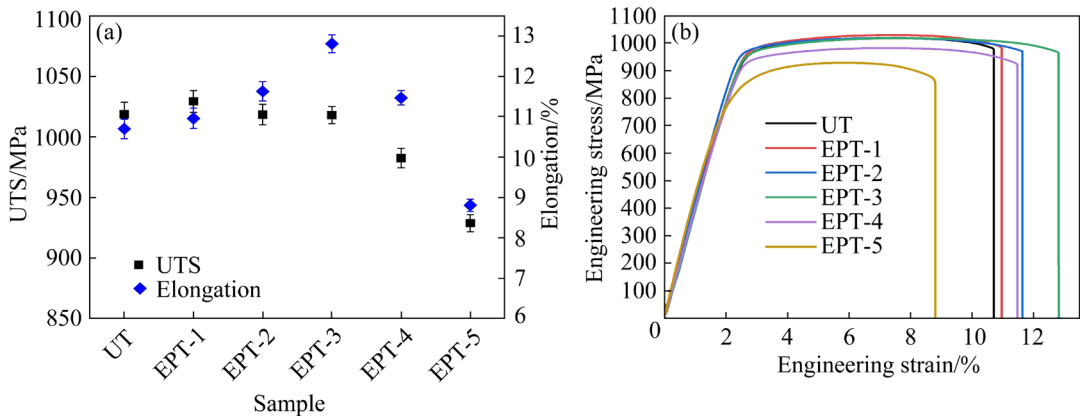

Fig. 3 Tensile properties of TC4 samples: (a) Variations for UTS and elongation; (b) Engineering stress−strain curves

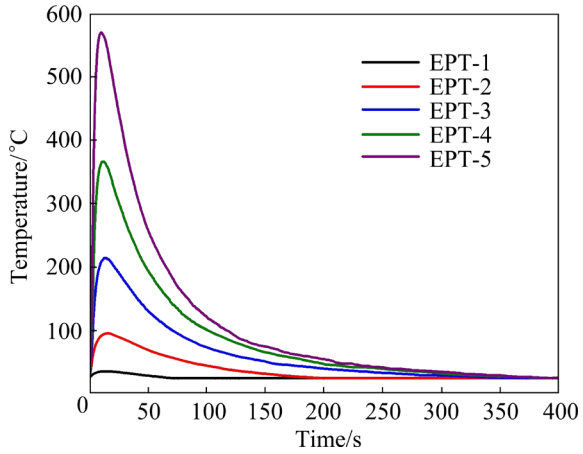

Fig. 4 Temperature on surface of TC4 samples with different treatments

temperature and cannot be measured directly by the transducer, it is estimated to follow a pattern similar to that reflected in Fig. 4 [17].

3.3 Fracture morphologies

Due to the apparent differences in UTS and elongation among UT, EPT-3, EPT-4, and EPT-5 samples presented in Fig. 3, the corresponding fractures of these tensile samples were selected to analyze fracture morphologies. Their morphologies in specific areas are presented in Fig. 5.

The samples, except for EPT-5, consist of tearing ridges and massive dimples, which belong to a typical ductile fracture mode. The depths of dimples in the fibrous zones of these samples are barely distinguishable, but dimples in the shear lip zone of the EPT-3 sample appear to be deeper. Equally importantly, more cracks can be seen in this zone, intuitively reflecting that ductile deformation in the EPT-3 sample is more pronounced than that in the other samples. For the EPT-4 fracture sample, the number of tearing ridges in the shear lip zone increases. In Fig. 5(d), the ridges are seen to spread

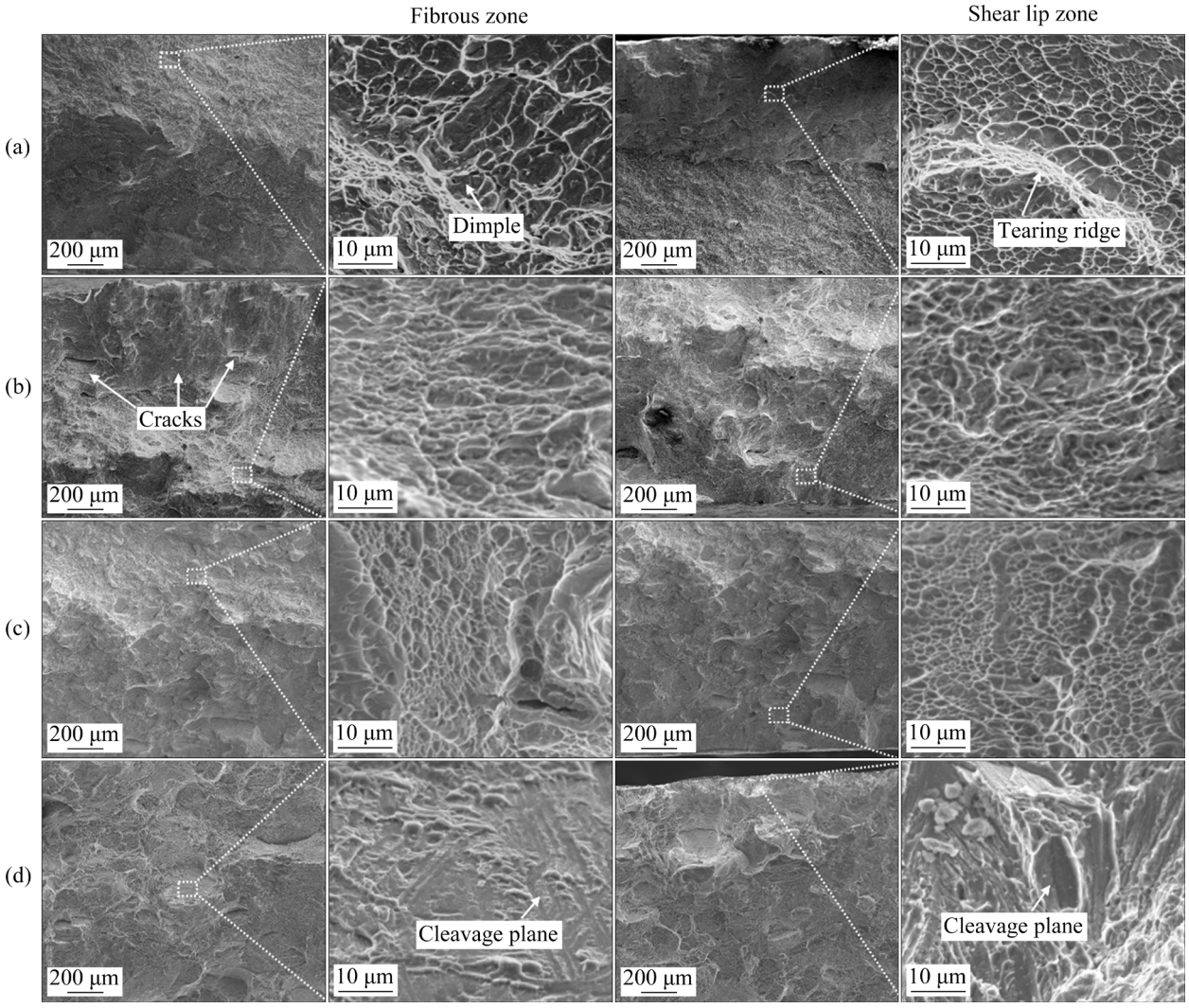

Fig. 5 Fracture surfaces for TC4 samples: (a) UT; (b) EPT-3; (c) EPT-4; (d) EPT-5

into another zone, which creates a stepped topography. Simultaneously, cleavage planes are included in the EPT-5 sample. These features indicate that brittle fracture occurred in the tensile sample, which accounts for its inferior tensile properties shown in Fig. 3.

3.4 Microstructure evolution

To understand the role of the pulse current in the tensile properties of the alloy, microstructure observation was carried out. The optical microscopy images of the selected samples are shown in Fig. 6.

Samples from UT to EPT-4 contain profuse lath structures dominated by the α phase. In the sample processed at 30 A/mm^2 (EPT-3), the lath structure expands slightly. Combined with the results in Fig. 3(a), this likely indicates that the magnitude of current density is moderate. As the current density continues to increase, the content of the coarse structure, presented in Fig. 6(c), exceeds a certain threshold, reducing the ductility of the alloy. At the highest current density (50 A/mm^2), the microstructure is mainly characterized by α' phase with a remarkable transition [17]. As illustrated in Figs. 3(a) and 6(d), the α' phase is responsible for the poor tensile properties of the EPT-5 tensile sample.

To further investigate the fracture behavior shown in Fig. 5, the longitudinal section of each tensile fracture was observed, and the results are presented in Fig. 7.

In the fibrous zones of the fracture samples (Figs. 7(a_2), (b_2), and (c_2)), the distributions and widths of α lath structures are similar. In the shear lip zone, however, the morphology of the EPT-3 sample differs from that of the other samples. As depicted in Figs. 7(b_1) and (b_3), there are notable lath structure twisting and widely distributed voids between slip bands in this zone. This morphology manifests an enhanced plastic deformation that is correlated with the deeper dimples presented in Fig. 5(b) [18]. As given in Figs. 7(d_2) and (d_3), the voids and deformed α' structures are similar to those of the EPT-3 sample in Figs. 7(b_2) and (b_1), respectively. The martensitic laths can disrupt the trade-off between tensile strength and ductility in the titanium alloy [19]. However, it is speculated that this structure, longer than that reported by YAO et al [19], accelerated the fracture progression of the EPT-5 sample. Furthermore, the α' structures displayed in Figs. 7(d_1−d_3) are coarser than the α structures in other fracture samples. This potentially

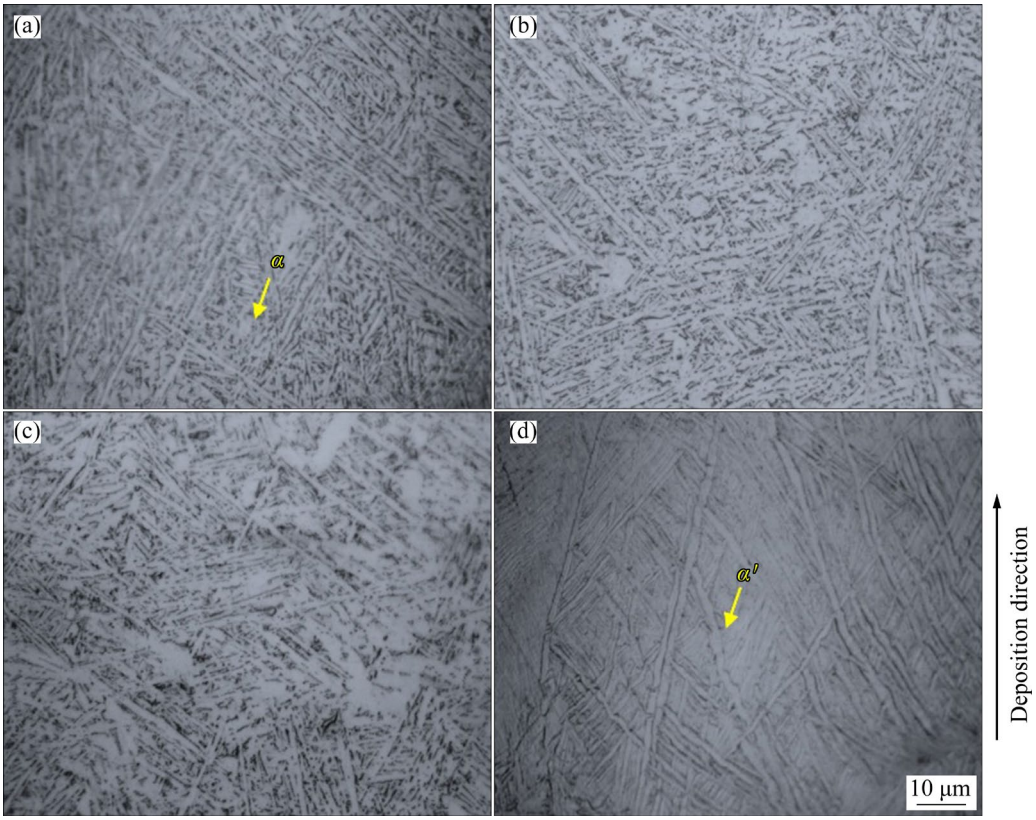

Fig. 6 Optical micrographs of TC4 samples: (a) UT; (b) EPT-3; (c) EPT-4; (d) EPT-5

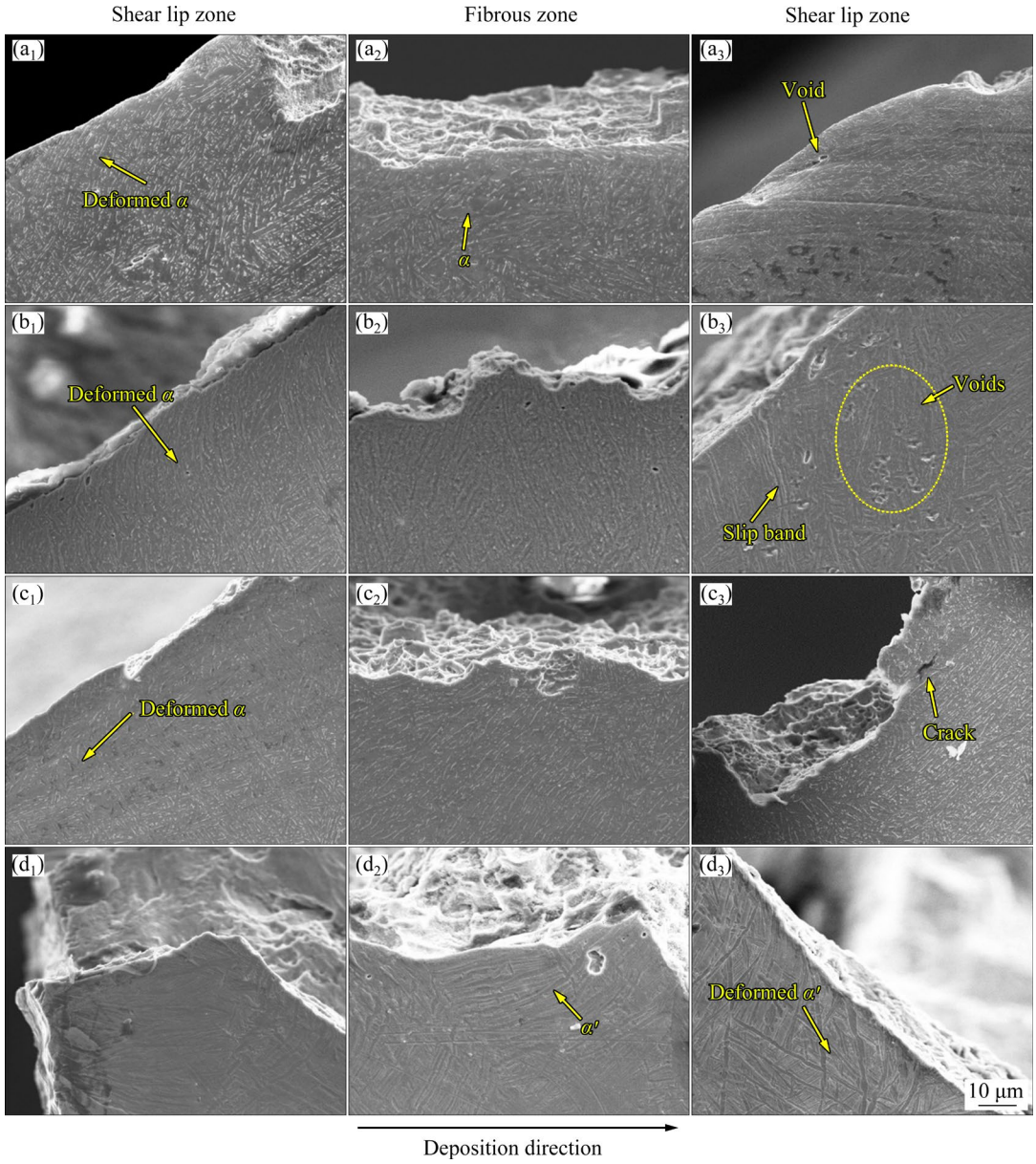

Fig. 7 Fracture morphologies on longitudinal sections of TC4 samples: (a_1−a_3) UT; (b_1−b_3) EPT-3; (c_1−c_3) EPT-4; (d_1−d_3) EPT-5

explains the inferior resistance to tensile deformation of the EPT-5 sample [20]. By comparing these deformation behaviors, it is further demonstrated that the EPT-3 sample exhibits excellent ductility.

To further investigate the effect of electro-pulsing on the alloy, samples (UT, EPT-3 and EPT-5) were selected for characterization of EBSD and TEM.

The change in tensile property induced by electro-pulsing generally originates from grain boundaries (GBs) and grain size, where GBs were characterized by misorientation angles. The grain morphologies of TC4 samples, along with the corresponding statistical results, are shown in Fig. 8.

It can be seen from Fig. 8(a) that the UT sample contains a plethora of low-angle grain boundaries (<15°, LAGBs). This phenomenon arises from the rapid remelting and solidification in the process of SLM, preventing complete recrystallization in a material [21]. Despite annealing the material in this study, the LAGBs in the alloy are not fully diminished. Conversely, there are fewer LAGBs in the EPT-3 sample. Figure 8(d) shows that the fraction of high-angle grain boundaries

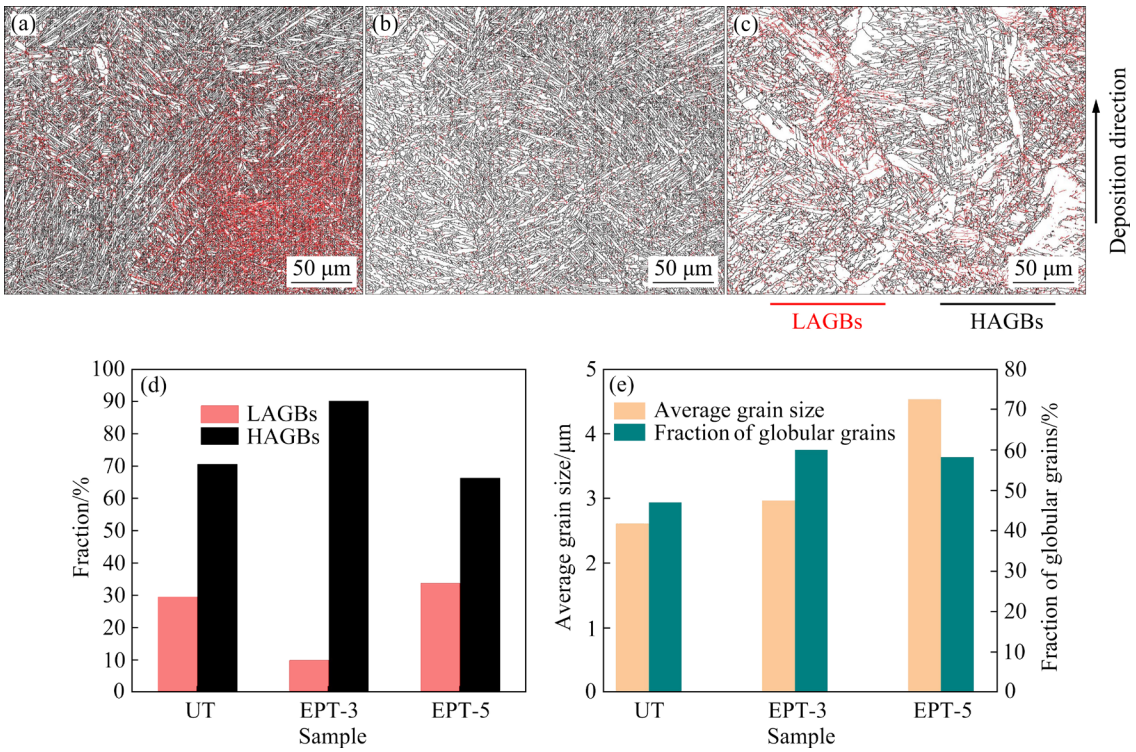

Fig. 8 Grain morphologies of TC4 samples of UT (a), EPT-3 (b), and EPT-5 (c), corresponding statistic results of GB angle (d), and average grain size and fraction of globular grains (e)

(>15°, HAGBs) in the EPT-3 sample approaches 90%, which is 27.74% higher than that in the UT sample. However, the HAGBs fraction in the EPT-5 sample is the lowest among these samples. As illustrated in Fig. 8(e), the average grain size of the EPT-3 sample is 13.79% larger than that of the UT sample. In comparison, the average grain size of the EPT-5 sample is the highest among the samples, implying that noticeable grain growth occurred. It is generally accepted that a grain with an aspect ratio of less than 2.5 satisfies the requirement of globularization [22]. As shown in Fig. 8(e), the EPT-3 sample has the highest fraction of globular grains. Although the fraction for the EPT-5 sample falls between those of the other samples, the highly coarse grains can degrade the GB strength and accelerate the tensile fracture [23]. As a result, the specific grain morphology and distribution of GBs in the EPT-3 sample facilitated greater plastic deformation accommodation and hindered crack propagation [24,25].

It has been revealed that electro-pulsing can enhance external energy, overcoming an energy barrier and inducing GB migration [26−28]. This requires sufficient conduction time and current density [26−28]. The pulse width in this work is millisecond-grade, which is higher than that in the previous studies [15]. Accordingly, the conduction time of each sample is estimated to be adequate. Besides, an electro-pulsing with high current density is responsible for the grain refinement in a metal [29]. Compared with the high current density from SONG et al [29], the current densities of EPT-3, 4, and 5 are far from adequate to refine the grains in the TC4 alloy. As the current density increases, the GB migration will induce more evident grain growth, namely, the expansion of the α structure (Figs. 6(c) and 7(c_1−c_3)). At the maximum current density, however, the grain growth will evolve into an evident phase transition (Figs. 6(d) and 7(d_1−d_3)).

It has been reported that drifting electrons can transfer energy to atoms through direct collision, creating a heat source that makes for atom diffusion [28,30]. During particle movement, the relationship between the GB migration and current density J_m can be expressed as [28,30]

$$Q=Q_t+Q_a=\frac{\pi GbD}{(1-v)k_BT(t)}+\frac{2NDZ^*erJ_mf\tau_p}{\pi k_BT(t)} \quad (1)$$

$$Q_m=C_0Q_a \quad (2)$$

$$Q_m=v_a/\Omega_a \quad (3)$$

$$v_{EPT}=v_t+v_a \quad (4)$$

where Q is the total atomic flux contributed by EPT; Q_t and Q_a are the atomic diffusion fluxes due to thermal and athermal effects, respectively; G is the shear modulus; b is the magnitude of Burgers vector; D refers to the lattice diffusion coefficient; v is the Poisson's ratio; k_B is the Boltzmann constant; $T(t)$ refers to the temperature during electro-pulsing processing; N is the atom density; Z^* is the effective valence; e is the charge on an electron; r is the electrical resistivity; f and τ_p denote the frequency and pulse width of electro-pulsing, respectively; Q_m represents the atomic diffusion flux across GBs; C_0 is the migration coefficient; Ω_a is the atom volume; v_{EPT} is the GB velocity during EPT; v_t and v_a are the GB migration velocity attributed to thermal and athermal effects, respectively.

Equations (1) to (4) indicate that electro-pulsing can enhance Q_a and v_a. In terms of thermal effect, D plays a crucial role in activating atomic motion, as it is primarily influenced by the temperature and exponentially increases with the rise of $T(t)$ [31]. Furthermore, the relationship between v_t, Q_t, and $T(t)$ indicates that the heat provided by the pulse current also promotes v_t [28,32]. With a moderate processing time, the average aspect ratio of the grains decreases to a certain degree, which can consume LAGBs and facilitate the structure in the EPT-3 sample [33].

Dislocations have been verified to respond to electro-pulsing [34]. Without visible plastic deformation in these selected samples, geometrically necessary dislocations (GNDs) generally evolve consistently with total dislocations [35]. Therefore, the GND density was employed to quantify the defect evolution, as presented in Fig. 9.

As can be seen from Fig. 9(a), there is a large number of dislocations in the UT sample, which stem from the inherent characteristics of SLM [4]. The repetitive heating and cooling in the manufacturing process gave rise to internal stresses, causing dislocations to accumulate and intertwine [36]. Figures 9(b) and (c) display an obvious reduction in the GND density compared with the UT sample. As shown in Fig. 9(d), the average GND density of EPT-3 sample is lower than that of the other samples. Moreover, the standard deviation of GND density in the EPT-3 sample is the lowest, manifesting a more homogeneous distribution of dislocations.

TEM bright field images showing dislocation morphologies of the TC4 samples are presented in Fig. 10. There are numerous dislocation tangles and zigzag dislocations in the UT sample. On the contrary, there are uniformly distributed dislocations without evident pile-ups in the EPT-3 sample. The

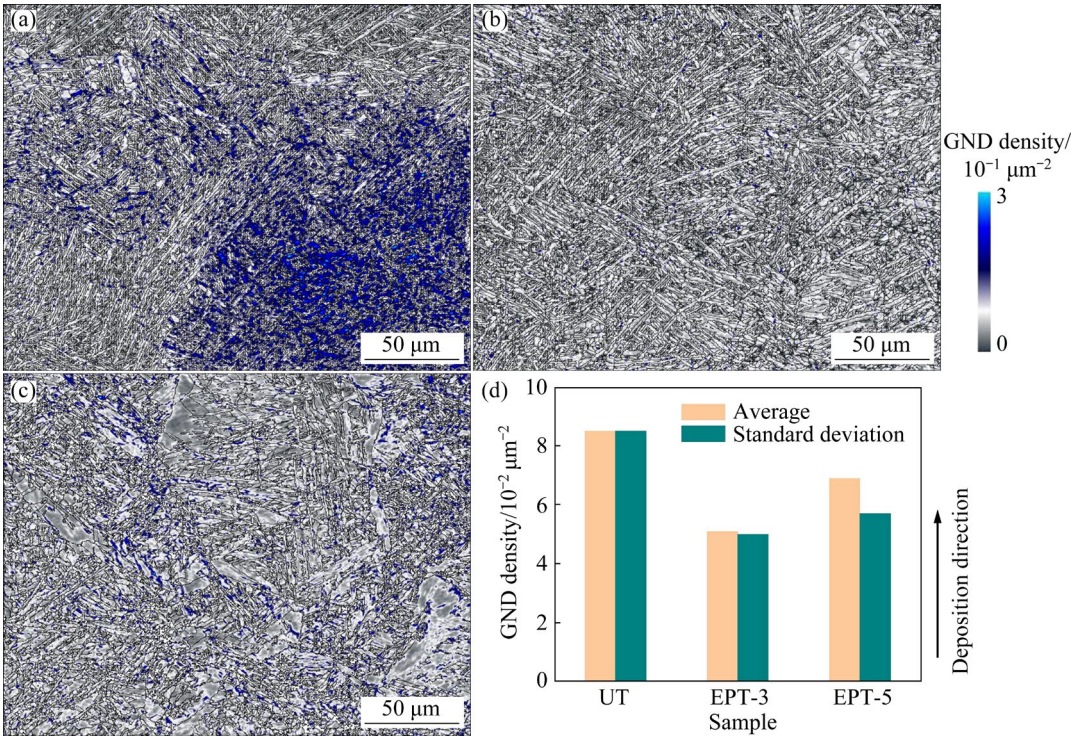

Fig. 9 GND maps of TC4 samples of UT (a), EPT-3 (b), and EPT-5 (c) with their statistic results (d)

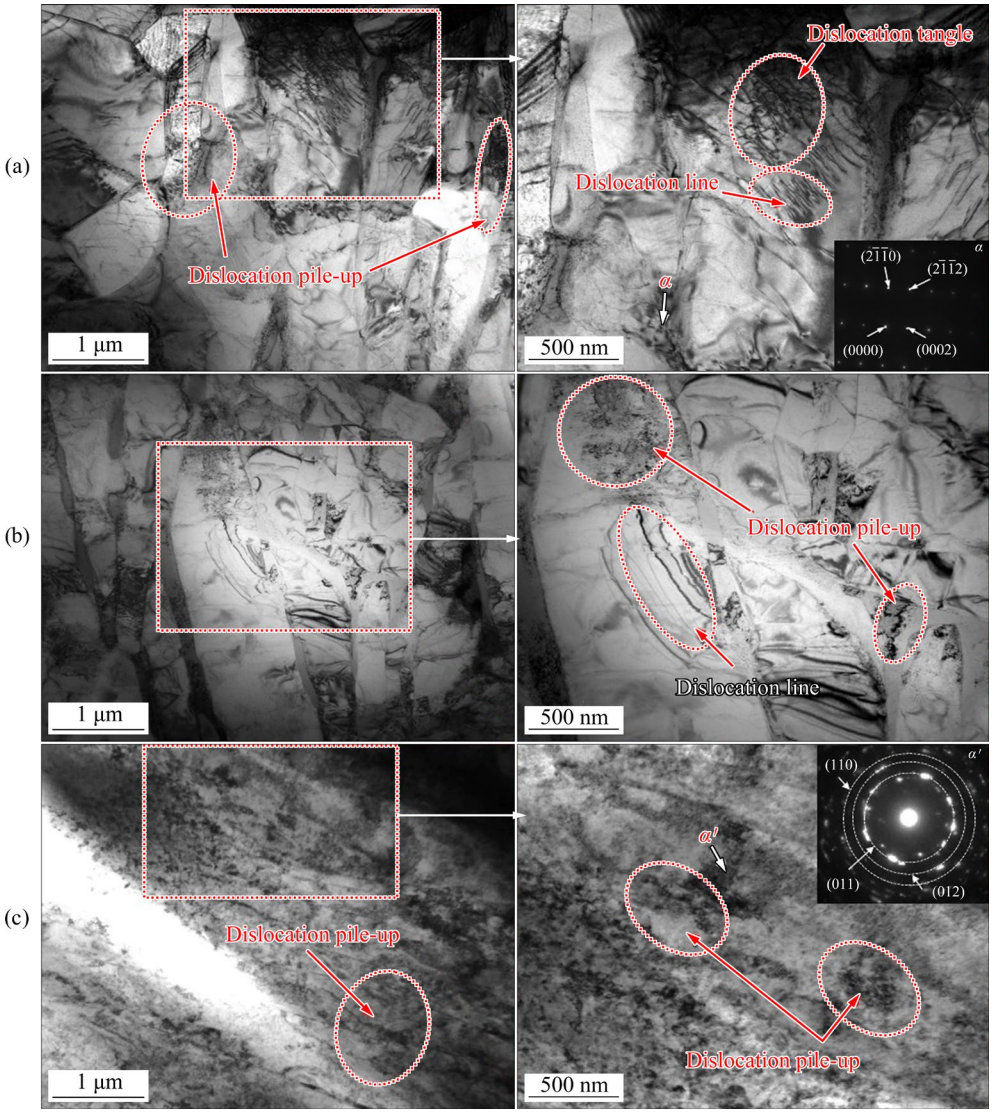

Fig. 10 TEM bright field images of TC4 samples: (a) UT; (b) EPT-3; (c) EPT-5 (SAED patterns inserted in (a) and (c) indicate the existence of α and α' phases, respectively)

dislocation pile-ups in the EPT-5 sample, however, are severer than those in the EPT-3 sample. Notably, the difference in the dislocation morphologies between these samples is consistent with that in the GND density.

The morphologies from Fig. 10 are conducive to different mechanical properties of the tensile samples. During the tensile deformation of the EPT-3 sample, it could be estimated that a continuous plastic flow was coordinated by dislocation with adequate space, helping to improve the elongation of the material [37]. It is noted that there is no evident decrease in tensile strength of the EPT-3 sample. This is owing to the dislocations with lower density and the slightly coarse α lath structures in the sample. However, for the EPT-5 sample, dislocation pile-ups near the GBs of the α' laths can be observed in Fig. 10(c), potentially weakening the GB strength and resulting in the inferior tensile strength [38]. Moreover, as calculated from Fig. 9(d), the GND density of the EPT-5 sample is 14% higher than that of the EPT-3 sample. This suggests that the heterogeneous and irregular dislocations can impair the ductility of the alloy [39,40].

It is proven that electro-pulsing can enhance the mobility of dislocations [41,42]. Furthermore, the current can generate additional energy near dislocations, reducing the threshold for dislocation motion and altering their density [15,26]. As new dislocations continuously form, they interact with the existing ones [43]. What's more, owing to the

current pulse width of this processing, some drifting electrons can be generated. With sufficient electrons and accumulated energy provided by available dislocations, dislocation annihilation can be activated, resulting in regularly distributed dislocations [40,44].

In addition to these factors discussed previously, the electron wind force should be considered to be responsible for dislocation motion [42]. In terms of the current density magnitude of EPT-3, indeed, the force is far from adequate, limiting its capacity to evacuate dislocation tangles and reduce the dislocation density [42]. Therefore, both drifting electrons and the additional energy can contribute to the dislocation evolution in the EPT-3 sample. By comparison, it can be estimated that the force produced by EPT-5 has been considerably increased [42]. However, EPT-5 can induce the highest temperature in the alloy (Fig. 4). This indicates that the thermal stress generated from the treatment is dominant, which can produce dislocations [38,44,45]. Furthermore, with the dislocation motion activated by the electropulsing [15], some dislocations migrate to the GBs of the α' laths, inducing the dislocation pile-ups as shown in Fig. 10(c). Thus, the thermal stress and dislocation motion account for the increase in dislocation density in the EPT-5 sample.

As can be characterized from the EBSD, the α phase constitutes 99.9% of the TC4 alloy. To discover the difference in α phase texture between the samples, pole figure (PF) and inverse pole figure (IPF) were applied in this characterization. The results are given in Fig. 11.

For the maximum intensity of each crystal plane texture (Figs. 11(a−c)), the intensity of {0001} basal texture is higher than that of other crystal plane

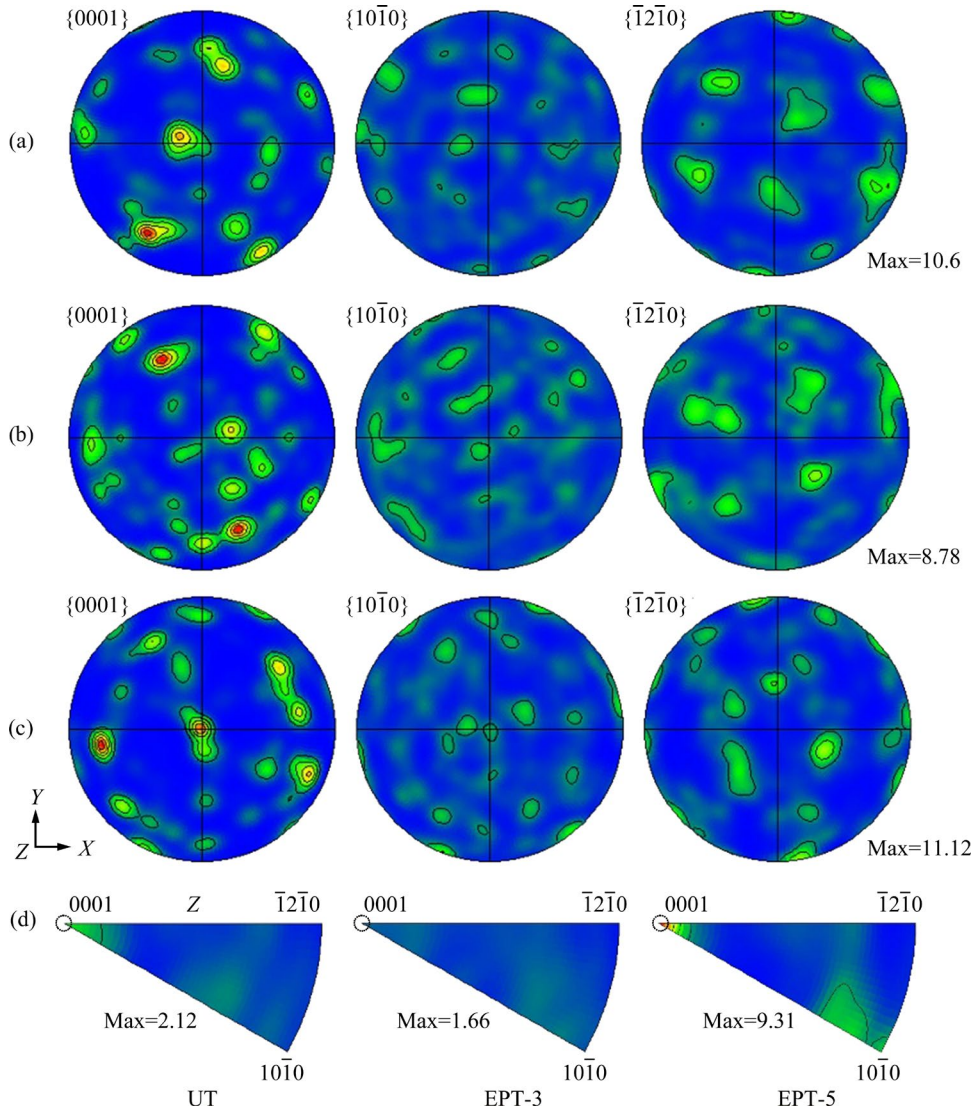

Fig. 11 PFs of α phase in TC4 samples of UT (a), EPT-3 (b), and EPT-5 (c) with corresponding IPFs in Z_0 direction (d)

groups. It is noted that the intensity of {0001} basal texture for the EPT-5 sample is the highest among the samples. This result signifies the improved anisotropy of the sample [46], but its plastic deformation capacity is generally restricted [47].

As shown in Fig. 11(d), the maximum texture intensity of each sample congregates in the [0001] corner. The [0001] orientation is parallel to the Z_0 direction, which corresponds to the direction of the tensile load. In particular, the intensity of the EPT-3 sample is lower than that of the other samples. This is because the fraction of basal planes perpendicular to the load is the smallest, which can delay fracture initiation during the load [46]. It is known that grains with basal planes are considered to be "hard grains" that resist dislocation slip during tensile deformation [48]. Therefore, based on the texture difference, EPT-3 is conducive to the better plastic deformation capacity of the alloy.

To delve deeper into the influence of the microstructure on the ductility, slip systems of samples subjected to different treatments have been evaluated. According to the results obtained from the EBSD, Schmid factor (SF) was utilized to assess the capacity of crystalline slip, and the relation is given by [49]

$$\varepsilon_{\mathrm{pl}} \propto \sigma_{\mathrm{cy}} \cdot M'^{2} \tag{5}$$

where $\varepsilon_{\mathrm{pl}}$ is the normal strain after an elastic stage, σ_{cy} is the calculated yield strength, and M' is the SF.

In general, an intergranular slip system in TC4 alloy is mainly composed of basal and prismatic slips [50]. Due to the anisotropy of the SLMed TC4 alloy, the basal slip takes precedence over the prismatic slip [51,52]. The SF distributions on both planes are exhibited in Fig. 12.

Figures 12(g) and (h) display the SF values of the slip system. For the basal slip, the EPT-5 sample

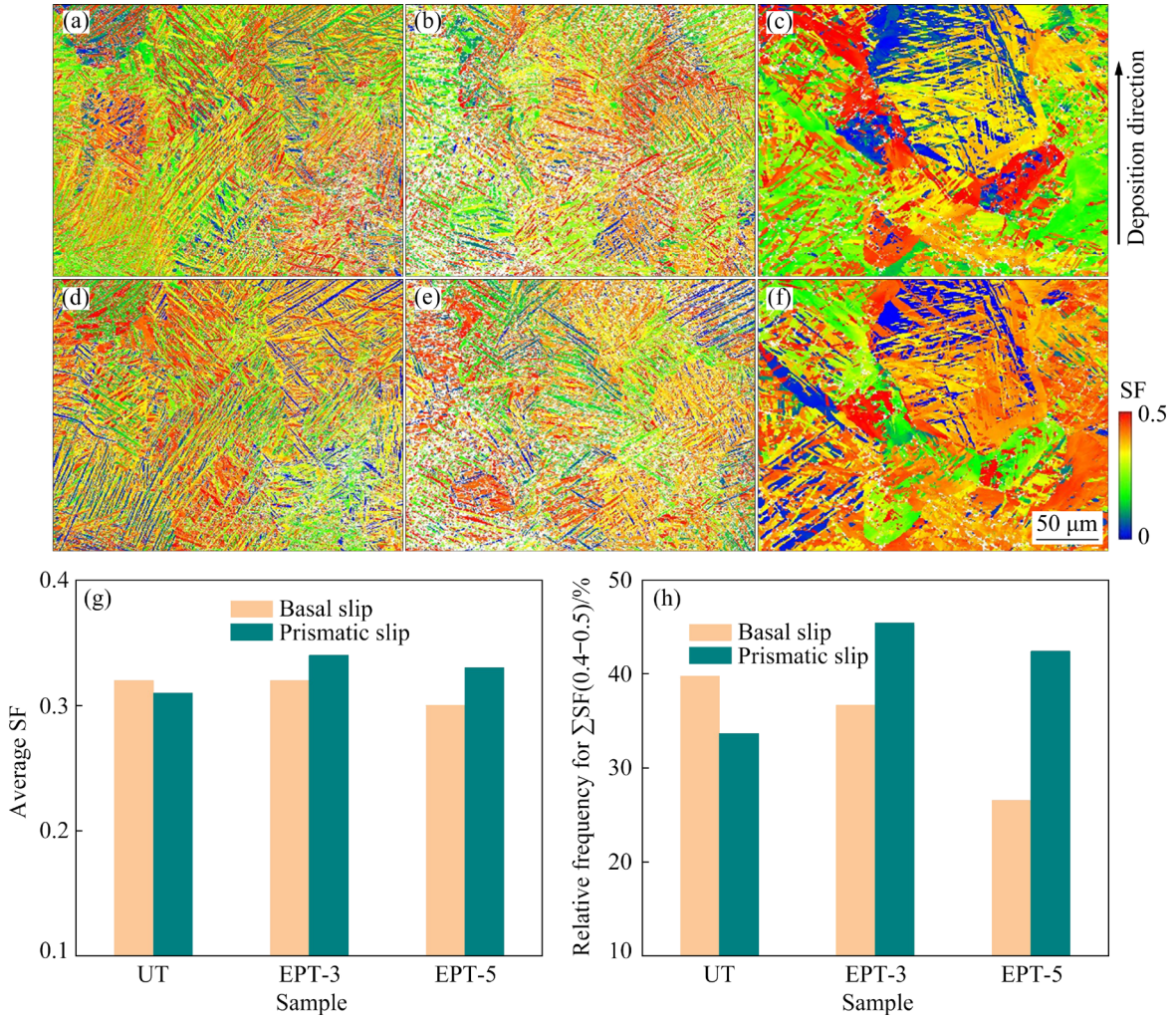

Fig. 12 Distribution maps of SF for TC4 samples of UT (a, d), EPT-3 (b, e), and EPT-5 (c, f) with corresponding statistical results (g, h)

has the lowest values of average SF and relative frequency of ΣSF(0.4−0.5). By comparison, for the prismatic slip, these values of the EPT-3 sample are notably higher than those of the other samples. Considering the differences in the grain size and dislocation distribution of both samples, these SF results suggest that the enhanced dislocation mobility with the optimal treatment promoted the excellent slip capacity of the planes [53]. Meanwhile, the distinctions in σ_{cy} between the tensile samples (UT and EPT-3) are less than 2%, which can be neglected. Therefore, the ε_{pl} increases with the proper application of electro-pulsing, which can promote crystalline slip and retard cracks originating from tensile stress [33]. With this increase, the ductility of the material can be considerably enhanced.

4 Conclusions

(1) According to the dependence of the tensile properties of the SLMed TC4 alloy on peak current density from electro-pulsing treatment (EPT), it is found that EPT-3 (30 A/mm^2) is the optimal treatment. This treatment allows the elongation of the alloy to become the highest.

(2) Based on the tensile fracture behaviors of all samples, features including deeper dimples, widely distributed voids, and more prominent slip bands suggest the excellent ductility of the EPT-3 sample.

(3) Grains and dislocations play an important role in the microstructural evolution during the optimal electro-pulsing (EPT-3). On the one hand, the HAGBs fraction is notably enhanced. Although the grain size increases, the increase is mild and is hardly detrimental to the tensile strength. On the other hand, the dislocations with lower density and higher distribution uniformity form. This noticeable evolution of the grains and dislocations can weaken the intensity of the {0001} basal texture. Particularly, the capacity of prismatic slip is improved, which can effectively delay tensile fracture. As a result, the interplay between these microstructural features elucidates the mechanism of ductility improvement.

CRediT authorship contribution statement

Zhen-shang HU: Writing − Original draft, Data curation, Investigation, Methodology, Funding acquisition; **Yi YANG:** Supervision, Data curation; **Ming-xia WU:** Writing − Review and editing, Supervision, Funding acquisition; **Ling XUE** and **Qiang LI:** Validation, Data curation; **Dong LU** and **Yong-sheng LIU:** Investigation, Resources.

Declaration of competing interest

The authors declare that they have no known competing financial interests or personal relationships that could have appeared to influence the work reported in this paper.

Acknowledgments

The authors wish to acknowledge the financial support from the National Natural Science Foundation of China (No. 52205490), and the Natural Science Foundation of Sichuan Province, China (No. 2022NSFSC0336).

References

[1] LIU S Y, SHIN Y C. Additive manufacturing of Ti−6Al−4V alloy: A review [J]. Materials & Design, 2019, 164(15): 107552.

[2] LAI Y, DENG Y, ZHU X W, GUO Y F, XU G F, HUANG J W, YIN Z M. Tensile property and microstructure of Al−4.77Mn−1.37Mg−0.67Sc−0.25Zr alloy under different selective laser melting processing parameters [J]. Transactions of Nonferrous Metals Society of China, 2023, 33(2): 357−370.

[3] YAP C Y, CHUA C K, DONG Z L, LIU Z H, ZHANG D Q, LIU L E, SING S L. Review of selective laser melting: Materials and applications [J]. Applied Physics Reviews, 2015, 2(4): 041101.

[4] ZHANG J Q, LIU Y, SHA G, JIN S B, HOU Z Y, BAYAT M, YANG N, TAN Q Y, YIN Y, LIU S Y, HATTEL J H, DARGUSCH M, HUANG X X, ZHANG M X. Designing against phase and property heterogeneities in additively manufactured titanium alloys [J]. Nature Communications, 2022, 13(1): 4660.

[5] SUN W B, MA Y E, HUANG W, ZHANG W H, QIAN X D. Effects of build direction on tensile and fatigue performance of selective laser melting Ti−6Al−4V titanium alloy [J]. International Journal of Fatigue, 2020, 130: 105260.

[6] BAGEHORN S, WEHR J, MAIER H J. Application of mechanical surface finishing processes for roughness reduction and fatigue improvement of additively manufactured Ti−6Al−4V parts [J]. International Journal of Fatigue, 2017, 102: 135−142.

[7] BENEDETTI M, TORRESANI E, LEONI M, FONTANARI V, BANDINI M, PEDERZOLLI C, POTRICH C. The effect of post-sintering treatments on the fatigue and biological behavior of Ti−6Al−4V ELI parts made by selective laser melting [J]. Journal of the Mechanical Behavior of Biomedical Materials, 2017, 71: 295−306.

[8] YAN X C, YIN S, CHEN C Y, HUANG C J, BOLOT R, LUPOI R, KUANG M, MA W Y, CODDET C, LIAO H L, LIU M. Effect of heat treatment on the phase transformation and mechanical properties of Ti−6Al−4V fabricated by

selective laser melting [J]. Journal of Alloys and Compounds, 2018, 764: 1056−1071.

[9] ZHOU C, ZHAN L H, LI H, ZHAO X, CHEN F, HUANG M H. Creep ageing behaviour assisted by electropulsing under different stresses for Al−Cu−Li alloy [J]. Transactions of Nonferrous Metals Society of China, 2021, 31(7): 1916−1929.

[10] SONG H, WANG Z J, GAO T J. Effect of high density electropulsing treatment on formability of TC4 titanium alloy sheet [J]. Transactions of Nonferrous Metals Society of China, 2007, 17(1): 87−92.

[11] ROSS C D, KRONENBERGER T J, ROTH J T. Effect of DC on the formability of Ti−6Al−4V [J]. Journal of Engineering Materials and Technology, 2009, 131(3): 031004.

[12] GAO L L, LIU J X, CHENG X W, LI S K, LUO Y M, GUO Q W. Effects of short time electric pulse heat treatment on microstructures and mechanical properties of hot-rolled Ti−6Al−4V alloy [J]. Materials Science and Engineering: A, 2014, 618: 104−111.

[13] ZHAO Z Y, WANG G F, HOU H L, HAN B S, ZHANG Y L, ZHANG N. Influence of high-energy pulse current on the mechanical properties and microstructures of Ti−6Al−4V alloy [J]. Journal of Materials Engineering and Performance, 2017, 26(10): 5146−5153.

[14] ZHAO Y X, PENG L F, LAI X M. Influence of the electric pulse on springback during stretch U-bending of Ti−6Al−4V titanium alloy sheets [J]. Journal of Materials Processing Technology, 2018, 261: 12−23.

[15] GAO J B, BEN D D, YANG H J, MENG L X, JI H B, LIAN D L, CHEN J, YI J L, WANG L, LI P. Effects of electropulsing on the microstructure and microhardness of a selective laser melted Ti−6Al−4V alloy [J]. Journal of Alloys and Compounds, 2021, 875: 160044.

[16] SHENG Y YI, HUA Y L, WANG X J, ZHAO X Y, CHEN L X, ZHOU H Y, WANG J, CHRISTOPHER B, LI W. Application of high-density electropulsing to improve the performance of metallic materials: Mechanisms, microstructure and properties [J]. Materials (Basel), 2018, 11(2): E185.

[17] HUANG J H, XU Z T, DENG Y J, PENG L F. Electropulsing-induced α to β phase transformation of Ti−6Al−4V [J]. Journal of Manufacturing Science and Engineering, 2019, 141(11): 111012.

[18] WANG J, ZHAO Y Q, ZHOU W, ZHAO Q Y, LEI C, ZENG W D. In-situ study on tensile deformation and damage evolution of metastable β titanium alloy with lamellar microstructure [J]. Materials Science and Engineering A, 2021, 824: 141790.

[19] YAO Z F, JIA X, YU J X, YANG M J, HUANG C, YANG Z J, WANG C P, YANG T, WANG S, SHI R P, WEI J, LIU X J. Rapid accomplishment of strength/ductility synergy for additively manufactured Ti−6Al−4V facilitated by machine learning [J]. Materials & Design, 2023, 225: 111559.

[20] FAN S J, HE B, LIU M S. Effect of pulse current density on microstructure of Ti−6Al−4V alloy by laser powder bed fusion [J]. Metals, 2022, 12(8): 1327.

[21] LI M, WU X, YANG Y, WEI Q S, YAN C Z, CAI C, LIU J, LI W, SHI Y S. TiAl/RGO (reduced graphene oxide) bulk composites with refined microstructure and enhanced nanohardness fabricated by selective laser melting (SLM) [J]. Materials Characterization, 2018, 143: 197−205.

[22] XU J W, ZENG W D, JIA Z Q, SUN X, ZHOU J H. Static globularization kinetics for Ti-17 alloy with initial lamellar microstructure [J]. Journal of Alloys and Compounds, 2014, 603: 239−247.

[23] PAN Z Q, ZHANG H O, SONG X L, WANG G L, WU C D, LIU X W. Influence of micro-rolling on the strength and ductility of plasma-arc additively manufactured Ti−6Al−4V alloys [J]. Journal of Materials Research and Technology, 2022, 21: 465−473.

[24] WEI L, XU X F, ZHAO Y, ZHOU Y C, YAN X D, WU Z C, YU Y Q, WU C. A shortened process of tri-modal microstructure developing in Ti−6Al−4V alloy via electropulsing-induces grain spheroidization [J]. Materials Characterization, 2023, 205: 113260.

[25] XIAO Y S, LAN L, GAO S, HE B, RONG Y H. Mechanism of ultrahigh ductility obtained by globularization of αGB for additive manufacturing Ti−6Al−4V [J]. Materials Science and Engineering: A, 2022, 858: 144174.

[26] HAN K, QIN S X, LI H P, LIU J, WANG Y, ZHANG C C, ZHANG G P, ZHANG S, ZHANG H B, ZHOU H P. EBSD study of the effect of electropulsing treatment on the microstructure evolution in a typical cold-deformed Ni-based superalloy [J]. Materials Characterization, 2019, 158: 109936.

[27] GUO H J, ZENG X, FAN J F, ZHANG H, ZHANG Q, LI W G, DONG H B, XU B S. Effect of electropulsing treatment on static recrystallization behavior of cold-rolled magnesium alloy ZK60 with different reductions [J]. Journal of Materials Science & Technology, 2019, 35(6): 1113−1120.

[28] ZHAO Z J, TO S, YIP W S, ZHUANG Z X. A rapid method for grain growth of Ti−6Al−4V alloy and its machinability [J]. The International Journal of Advanced Manufacturing Technology, 2019, 104(5): 2347−2361.

[29] SONG H, WANG Z J, HE X D. Improving in plasticity of orthorhombic Ti_2AlNb-based alloys sheet by high density electropulsing [J]. Transactions of Nonferrous Metals Society of China, 2013, 23(1): 32−37.

[30] KIM M, LEE S H, YU J, CHEON S, BYUN S, LEE C S, LEE T. Enhanced kinetics of microstructural evolution in Ti−6Al−4V through electropulsing treatment [J]. Journal of Materials Research and Technology, 2023, 26: 8500−8508.

[31] JIANG Y B, TANG G Y, SHEK C H, LIU W. Microstructure and texture evolution of the cold-rolled AZ91 magnesium alloy strip under electropulsing treatment [J]. Journal of Alloys and Compounds, 2011, 509(11): 4308−4313.

[32] ZHU J, LIU S, LIN Y, WANG G C. Effect of electropulsing on microstructure and properties of severely plastically deformed pure copper sheet [J]. Journal of Materials Engineering and Performance, 2020, 29(8): 841−848.

[33] LIU Z G, LI P J, XIONG L T, LIU T Y, HE L J. High-temperature tensile deformation behavior and microstructure evolution of Ti55 titanium alloy [J]. Materials Science and Engineering A, 2017, 680(5): 259−269.

[34] ZHAO Z J, TO S, SUN Z W, JI R J, YU K M. Microstructural effects of Ti−6Al−4V alloys modified by electropulsing treatment on ultraprecision diamond turning [J]. Journal of Manufacturing Processes, 2019, 39: 58−68.

[35] ZHANG Y Q, NGAN A H W. Extracting dislocation microstructures by deep learning [J]. International Journal of Plasticity, 2019, 115: 18−28.

[36] WU W Q, ZHOU R, WEI B Q, NI S, LIU Y, SONG M. Nanosized precipitates and dislocation networks reinforced C-containing CoCrFeNi high-entropy alloy fabricated by selective laser melting [J]. Materials Characterization, 2018, 144: 605−610.

[37] XIAO A, YAN Z Q, HUANG C Q, YU Z X, WANG S P, CUI X H. Reduction of springback of Ti−6Al−4V alloy by high-density and instantaneous pulsed current [J]. Materials Science and Engineering: A, 2023, 877(22): 145188.
[38] LIU C, XIE L C, QIAN D S, HUA L, WANG L Q, ZHANG L C. Microstructure evolution and mechanical property response of TC11 titanium alloy under electroshock treatment [J]. Materials & Design, 2021, 198: 109322.
[39] TONG Z P, WAN W B, LIU H L, ZHOU W F, YE Y X, REN X D. Combination of annealing and laser shock peening for tailoring microstructure and mechanical properties of laser directed energy deposited CrMnFeCoNi high-entropy alloy [J]. Additive Manufacturing, 2023, 61: 103345.
[40] WANG Y T, ZHAO Y G, PAN D, XU X F, CHONG X Y, YIN P L. Multiple precipitates and weakened PLC effect in the electro-pulsing treated Al−Mg−Si alloy [J]. Materials Letters, 2020, 261: 127089.
[41] LU W J, QIN R S. Stability of martensite with pulsed electric current in dual-phase steels [J]. Materials Science and Engineering: A, 2016, 677: 252−258.
[42] ZHANG J T, LIU Z H, SUN J X, ZHAO H L, SHI Q Y, MA D W. Microstructure and mechanical property of electropulsing tempered ultrafine grained 42CrMo steel [J]. Materials Science and Engineering: A, 2020, 782: 139213.
[43] WANG Y T, ZHAO Y G, XU X F, PAN D, JIANG W Q, YANG X H, WANG Z. Superior mechanical properties induced by the interaction between dislocations and precipitates in the electro-pulsing treated Al−Mg−Si alloys [J]. Materials Science and Engineering: A, 2018, 735: 154−161.
[44] YIN P L, ZANG H B, ZHAO Y G, WU C, XU X F, PAN D, JIANG W Q. Superior mechanical properties of 40Cr steel obtained by quenching and microstress relieving under electropulsing [J]. Materials Science and Engineering: A, 2020, 772: 138782.
[45] PAN D, WANG Y T, GUO Q T, ZHANG D, XU X F, ZHAO Y G. Grain refinement of Al−Mg−Si alloy without any mechanical deformation and matrix phase transformation via cyclic electro-pulsing treatment [J]. Materials Science and Engineering A, 2021, 807: 140916.
[46] XU S, ZHANG H M, XIAO N M, QIU R S, CUI Z S, FU M W. Mechanisms of macrozone elimination and grain refinement of near α Ti alloy via the spheroidization of the Widmannstätten structure [J]. Acta Materialia, 2023, 260: 119339.
[47] GUAN L, TANG G Y, JIANG Y B, CHU P K. Texture evolution in cold-rolled AZ31 magnesium alloy during electropulsing treatment [J]. Journal of Alloys and Compounds, 2009, 487(1/2): 309−313.
[48] BHANDARI L, GAUR V. Different post-processing methods to improve fatigue properties of additively built Ti−6Al−4V alloy [J]. International Journal of Fatigue, 2023, 176: 107850.
[49] PAN D, ZHAO Y G, XU X F, WANG Y T, JIANG W Q, CHONG X Y. A novel strengthening and toughening strategy for T250 maraging steel: Cluster-orientation governed higher strength-ductility combination induced by electropulsing [J]. Materials and Design, 2019, 169: 107686.
[50] ZAEFFERER S. A study of active deformation systems in titanium alloys: dependence on alloy composition and correlation with deformation texture [J]. Materials Science and Engineering: A, 2003, 344(1/2): 20−30.
[51] MUIRURI A, MARINGA M, PREEZ W D. Statistical analysis of the distribution of the schmid factor in as-built and annealed parts produced by laser powder bed fusion [J]. Crystals, 2022, 12(5): 743.
[52] WANG F B, LIU Y K, TONG Y X, ZHANG C, JIANG F C, WANG J D, Effect of electropulsing on anisotropy in strength of laser metal deposited Ti−6Al−4V alloy [J]. Transactions of Nonferrous Metals Society of China, 2022, 32(8): 2578−2586.
[53] WANG W R, YUAN L H, WEI Z L, ZHANG H, ZHANG W F. Cold-rolled Ti−Al−V−Zr−Fe titanium alloy tubing with outstanding tensile properties [J]. Journal of Alloys and Compounds, 2023, 931: 167558.

脉冲电流处理对 SLM 成形 TC4 钛合金拉伸性能及显微组织的影响

胡臻尚[1]，杨 屹[1]，吴明霞[1]，薛 令[1]，李 强[1]，卢 东[2,3]，刘永胜[2,3]

1. 四川大学 机械工程学院，成都 610065；
2. 成都市先进金属材料工业技术研究院有限公司 四川省先进金属材料增材制造工程技术研究中心，成都 610300；
3. 钒钛资源综合利用国家重点实验室(攀钢集团有限公司)，攀枝花 617000

摘 要：研究了具有不同峰值电流密度(J_m)的脉冲电流处理(EPT)对选择性激光熔化法(SLM)制备的 TC4 合金拉伸性能的影响，以实现该材料拉伸性能的显著改善。当 J_m 为 30 A/mm^2 时，伸长率显著提高了 19.72%，抗拉强度基本不变。这种良好的延展性在于断口表面具有较深的韧窝以及剪切唇区出现的裂纹。同时，该性能的改善体现在断口剖面出现了分布较广的孔洞和明显的滑移带。断裂行为的这些变化归因于良好的 EPT 工艺提高了大角度晶界含量，降低了位错密度。这种显微组织引起基面织构强度减弱，增强了对应滑移面的滑移能力，从而有利于提高材料的塑性形变能力。

关键词：脉冲电流处理；SLM 成形 TC4 钛合金；拉伸性能；断裂行为；显微组织

(Edited by Wei-ping CHEN)